



Three-dimensional roof collapse analysis in circular tunnels in rock

Dowon Park, Radoslaw L. Michalowski *

Department of Civil & Environmental Engineering, University of Michigan, 2028 G.G. Brown Bldg., Ann Arbor, MI, 48109-2125, USA

ARTICLE INFO

Keywords:

Tunnel roof stability
Rock engineering
Hoek-Brown strength criterion
Limit analysis

ABSTRACT

Collapse of a roof in circular cross-section tunnels is analyzed. The kinematic approach of limit analysis is utilized, with strength of the rock described by the Hoek-Brown failure criterion. The parametric form of the Hoek-Brown function is used to avoid introduction of an alternative explicit form of the shear strength criterion. Three measures of safety are considered: stability number, the factor of safety, and the support pressure needed to assure roof stability. The shape of the rock block in the failure mechanism consists of a right elliptic cone with a piece-wise linear generatrix and a prismatic section inserted between the two halves of the cone. The complexity of the cross-section of the block with the tunnel makes for an intricate integration of the rates of the dissipated work and the work of external forces. All three measures of safety are strongly dependent on the quality of rock described in the *Geological Strength Index*, whereas the dependence on the rock type captured in coefficient m_i is less distinct. The length of the roof failure mechanism is subject to a constraint dependent on the spacing of the supporting ribs in the tunnel. All measures of safety (or stability) are distinctly dependent on the length constraint; the shorter the spacing between the ribs, the safer the tunnel against roof collapse. The 2D analysis yields the most conservative outcome.

1. Introduction

Construction and operation of tunnels are among the challenges in the development of transportation infrastructure. Collapse of the tunnel roof is among the more common types of failure, both during construction and during service. While available two-dimensional (2D) analyses can provide conservative estimates of the roof safety,^{1–3} more accurate three-dimensional (3D) analyses pose a challenge, because of the complex geometry of the failure zone, exacerbated by the nonlinear pressure dependency of the rock shear strength.

Among the first analyses of tunnel roof stability was that of Lippmann,⁴ who applied limit analysis to a flat-ceiling tunnel in a rock with strength governed by the Mohr-Coulomb failure criterion. Since then, a number of analytical or numerical studies have been presented with 2D analyses for flat-ceiling or circular cross-section roofs.^{1–3,5–8} Three-dimensional stability analyses of tunnel roofs are not as common, because of their complexity, especially for tunnels with non-flat ceiling.

Tunnels in good quality rock typically have a continuous lining, but in variable rock or poor quality rock, periodic supports in the form of structural ribs may be installed. They may take the form of rolled steel sections or lattice girders combined with sprayed concrete. The presence of ribs will likely influence the potential failure mechanism by limiting

its length to the rib spacing. Such collapse mechanisms will have a 3D geometry and will necessitate a 3D analysis. Consideration of such mechanisms in design is likely to have a beneficial effect on the economics of tunnel construction.

Most contemporary tunnel construction procedures involve tunnel boring machines (TBM), which open a circular cross-section cavity in the rock. A roof collapse is possible behind the TBM during its operation, thus some TBMs are equipped with a roof shield protecting the crew and the machine. Consideration of roof collapse during both the tunnel construction and service requires a 3D analysis of the roof's stability. Attempts at the 3D analyses are scarce, and those available in the literature consider flat-ceiling tunnels. Yang and Huang⁹ extended Fraldi and Guarracino¹ plane-strain variational solution for tunnels with rectangular cross-sections. Huang et al.¹⁰ presented a 3D axi-symmetric generalization of a 2D analytical solution for circular tunnels suggested earlier by Fraldi and Guarracino.⁷ This solution, however, is applicable to spherical cavities, and not to tunnels with circular cross-sections, because the cross-section of the cylindrical tunnel surface with a surface of a right circular cone is not axisymmetric. Besides, the expectation that a 3D roof collapse of a long cavity (tunnel) should have axi-symmetric geometry is rather arbitrary. It might also be of interest that previous attempts focused on the shape of the block falling from the

* Corresponding author.

E-mail address: rlmich@umich.edu (R.L. Michalowski).

roof of a cavity, whereas this paper focuses on quantitative safety assessment measures, with the block shape definition being an intermediate step in the analysis.

In order to account for a complex cross-section of the falling rock block and the cylindrical surface of the tunnel, a semi-analytical method was devised. At the cost of an elaborate integration scheme, the intricate geometry was accounted for. The kinematic approach of limit analysis for rocks governed by the modified Hoek-Brown strength criterion¹¹ was used. It might be of interest that the analytical approaches used in earlier attempts^{1,9,10} all used an alternative form of the Hoek-Brown function with the shear strength being an explicit function of the normal stress. This is because the original form of the Hoek-Brown criterion is a function of the principal stresses, not convenient in variational limit analysis. To avoid this issue, a parametric form of the Hoek-Brown criterion is used in the approach presented in this paper.

The modified Hoek-Brown failure criterion for rocks is briefly reviewed in the next section, concluding with comments on applicability of limit analysis to rocks. The collapse mechanism is described, and the analysis is outlined as to how to calculate the three measures of safety (stability): the stability number, the factor of safety, and the minimum support pressure needed to render tunnels in weak rock stable. Numerical results are presented in charts and tables. The authors are not aware of any earlier studies reporting the quantitative safety measures for three-dimensional roof collapse mechanisms in rock governed by the Hoek-Brown failure criterion, in tunnels with circular cross-sections.

2. Hoek-Brown failure criterion for rocks

Various failure criteria have been suggested to describe the strength of rocks, e.g., Paul,¹² Bieniawski,¹³ Barton,¹⁴ and Hoek and Brown.¹⁵ Among those, the Hoek-Brown failure criterion became preferred by engineers over the alternatives, because of its empirical nature and its direct link to the quality, type, and state of the rock. A series of enhancements have been introduced into that criterion over the years, and they were summarized in a paper by Hoek and Marinos.¹⁶

2.1. Generalized Hoek-Brown strength criterion

The rock is considered isotropic, while the quality, the type of the rock, and its disturbance are considered through a relatively small number of parameters. The most recent version of this function¹¹ is often referred to as the *generalized* Hoek-Brown criterion, and it takes the following form

$$\sigma'_1 = \sigma'_3 + \sigma_{ci} \left(m_b \frac{\sigma'_3}{\sigma_{ci}} + s \right)^a \quad (1)$$

with the dimensionless material parameters defined as

$$m_b = m_i e^{\left(\frac{GSI-100}{28-14D} \right)} \quad (2)$$

$$a = \frac{1}{2} + \frac{1}{6} \left(e^{-\frac{GSI}{15}} - e^{-\frac{20}{3}} \right) \quad (3)$$

$$s = e^{\left(\frac{GSI-100}{9-3D} \right)} \quad (4)$$

where σ'_1 and σ'_3 are the major and minor effective principal stresses, σ_{ci} is the uniaxial compressive strength of intact rock, and *GSI* is the Geological Strength Index (typically in a range from 5 to 100). Parameter m_i depends on the rock type (typically in a range of 5–30), and *D* is the disturbance factor (in a range of 0–1). More detailed description of these properties and their estimates can be found elsewhere (Marinos and Hoek¹⁷ and Hoek et al.¹¹). The strength criterion in Eq. (1) can be

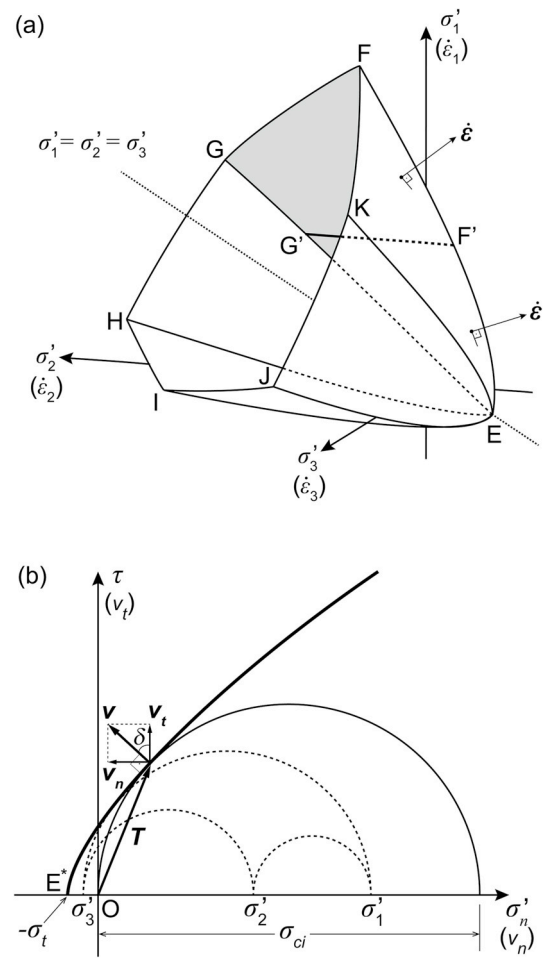


Fig. 1. The Hoek-Brown failure criterion: (a) failure surface in Haigh-Westergaard space, and (b) strength envelope in τ, σ_n plane, with three stress circles mapping a point from the failure surface in $\sigma'_1, \sigma'_2, \sigma'_3$ space.

represented as the EFG_E section of the failure surface in the Haigh-Westergaard space in Fig. 1(a), where $\sigma'_1 \geq \sigma'_2 \geq \sigma'_3$ (all effective stresses). The function in Eq. (1) is independent of intermediate principal stress σ'_2 ; therefore, axis σ'_2 must be parallel to surface EFG_E. Consequently, any plane from a pencil of planes through axis σ'_2 will form a straight-line cross-section with surface EFG_E, parallel to axis σ'_2 (for example, G'F').

Any point on surface EFG_E represents a limit-state combination of stresses σ'_1, σ'_2 and σ'_3 . Transformed onto a τ, σ_n plane, such a stress state is represented by three stress circles, as illustrated by the dashed semi-circles in Fig. 1(b). Defining a triaxial isotropic tensile strength as σ_t , and setting all principal stresses to $-\sigma_t$, all three stress circles reduce to one point at E*. The isotropic tensile strength is uniquely defined by the strength criterion in Eq. (1); substituting $\sigma'_1 = \sigma'_3 = -\sigma_t$ in Eq. (1), one obtains

$$\sigma_t = \frac{s\sigma_{ci}}{m_b} \quad (5)$$

Isotropic tensile strength σ_t is not necessarily equal to the one-dimensional or biaxial tensile strength, although, typically, it does not differ much (for minimally disturbed rocks, $D = 0$, the uniaxial tensile strength is smaller than σ_t , but the difference does not exceed 4%, and it is less than 1% for a large range of *GSI* and m_i).

2.2. Parametric form of the Hoek-Brown strength criterion

The Hoek-Brown criterion was developed as a function of the major and minor effective principal stresses. Some of the methods in geotechnical engineering and geomechanics call for a strength envelope expressed explicitly in terms of the traction components (τ, σ_n) on the failure surface. For that reason, previous attempts at stability analysis of cavities and tunnels in rocks^{1,9} did not use the original Hoek-Brown criterion in Eq. (1), but rather its approximation $\tau = f(\sigma_n)$ in the form

$$\tau = A\sigma_{ci} \left(\frac{\sigma_n + \sigma_i}{\sigma_{ci}} \right)^B \quad (6)$$

where A and B are the dimensionless parameters determined from the best fit into the H-B criterion in the range of interest. A function similar to that in Eq. (6) was suggested by Hoek and Brown as an alternative criterion form in their original paper.¹⁵ In this paper, we avoid using the approximate form in Eq. (6); instead, we utilize a parametric form of the criterion in Eq. (1). For this, rupture angle δ , shown in Fig. 1(b), is used as a parameter.¹⁸ Making use of the procedure in Balmer¹⁹ (see also Kumar²⁰), the components of the traction vector on the failure surface can be expressed as

$$\sigma_n = \sigma_{ci} \left\{ \left(\frac{1}{m_b} + \frac{\sin\delta}{m_b a} \right) \left[\frac{m_b a (1 - \sin\delta)}{2 \sin\delta} \right]^{\frac{1}{1-a}} - \frac{s}{m_b} \right\} \quad (7)$$

$$\tau = \sigma_{ci} \left\{ \frac{\cos\delta}{2} \left[\frac{m_b a (1 - \sin\delta)}{2 \sin\delta} \right]^{\frac{a}{1-a}} \right\} \quad (8)$$

The expressions in Eqs. (7) and (8) can now be used for varying parameter δ to find points on the strength envelope on plane τ, σ_n , identical to the envelope of all limit states expressed in terms of major and minor principal stresses σ'_1 and σ'_3 in Eq. (1).

3. Problem statement and the method of solution

3.1. Measures of roof safety

Three measures of roof safety are considered in this paper, the first being the *stability number*, defined as

$$N = \left(\frac{\sigma_{ci}}{\gamma R} \right)_{crit} \quad (9)$$

where σ_{ci} is the compressive strength of the intact rock, γ is its unit weight, and R is the radius of the tunnel cross-section. Stability number N is a dimensionless combination of the rock properties and the tunnel size for which the loss of stability can occur (critical combination). The safety margin of the tunnel against roof instability is reflected in the difference between the dimensionless group $\sigma_{ci}/\gamma R$ for an existing tunnel, referred to here also as the *characteristic strength number*, and its critical value N . Tunnels with a characteristic strength number larger than the stability number are safe against roof collapse, and the larger the difference, the larger the safety margin.

The second measure of safety considered is the *factor of safety*, defined as a ratio of the shear strength of the rock, τ , to the reduced value of the shear strength, τ_d , which is needed for the tunnel roof to maintain limit equilibrium (demand on shear strength)

$$F = \frac{\tau}{\tau_d} \quad (10)$$

This definition of the factor of safety is not commonly used for rocks with strength defined by non-linear envelopes in the τ, σ_n plane, because of some analytical intricacies. The factor of safety so defined is, effectively, a strength reduction factor, and it is demonstrated in this paper that this definition of the factor of safety can be used successfully for rocks with strength defined by the Hoek-Brown failure criterion.

The third measure of safety considered is the *critical supporting*

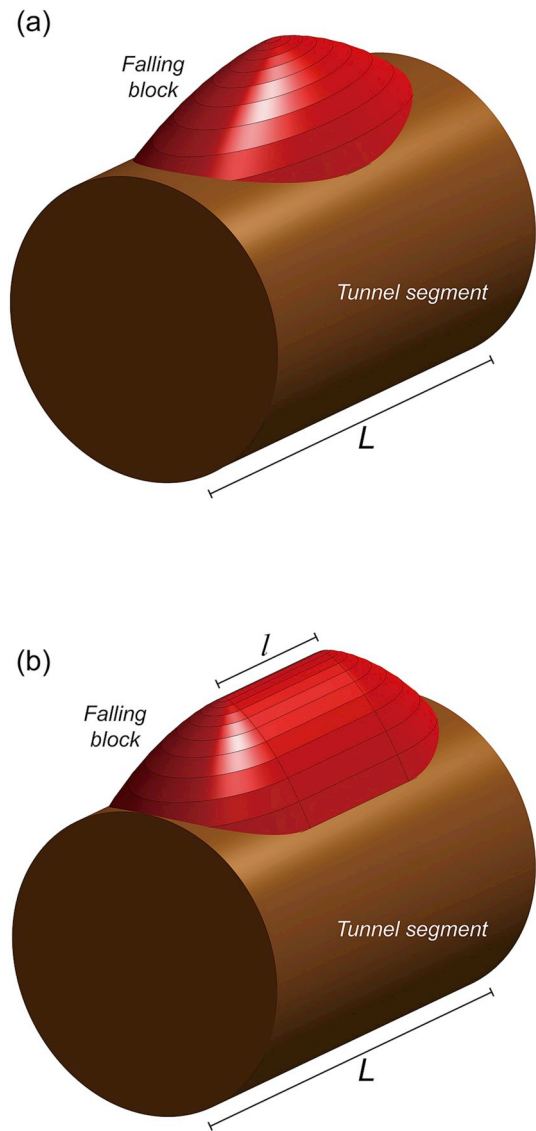


Fig. 2. A schematic of 3D roof failure surfaces: (a) right elliptic cone block intersecting the circular cross-section tunnel, and (b) right elliptic cone with a prismatic insert.

pressure, p (or its dimensionless form $p/\gamma R$). This supporting pressure is an induced reaction of the tunnel lining to the potentially collapsing rock block, and it will be assumed in the analysis as a fictitious, uniformly distributed pressure on the inside of the tunnel, necessary to prevent roof collapse in tunnels deemed unstable (when characteristic strength number $\sigma_{ci}/\gamma R$ is lower than the stability number in Eq. (9)).

3.2. Problem description

Roof stability in tunnels with a circular cross-section is considered. The tunnels considered are deep enough, so that the collapse mechanism does not propagate to the ground surface. This restriction can be easily removed as shown by Fraldi et al.,⁸ to make the method applicable to both deep and shallow tunnels. The strength of the rock is described by the Hoek-Brown failure criterion and the initial irreversible deformation is governed by the normality plastic flow rule. The tunnel lining is characterized by a ribbed structure, with a potential failure limited to sections between two neighboring ribs.

When calculating the stability number or the factor of safety, a stress-free boundary condition will be defined on the interior surface of the

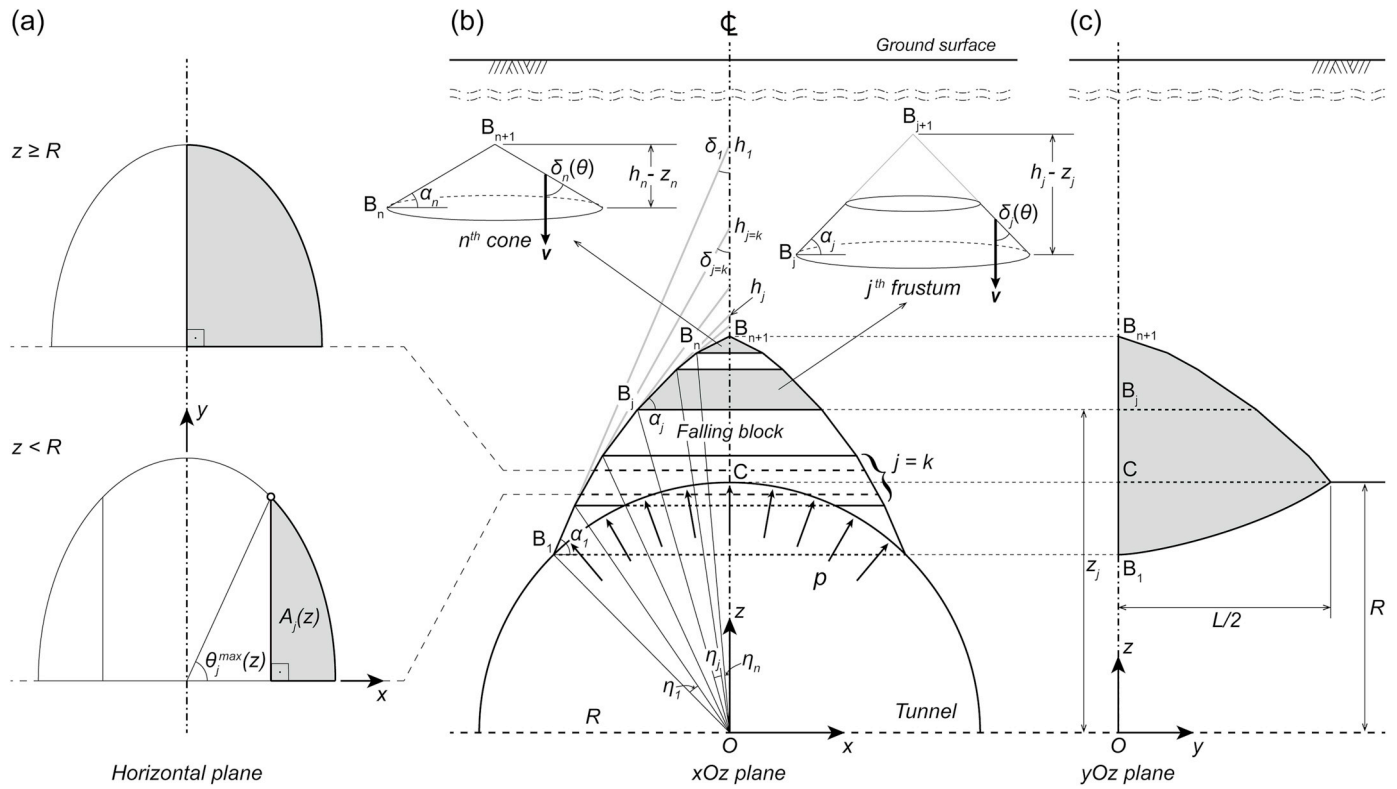


Fig. 3. A mechanism with piece-wise linear right elliptical cone block: (a) horizontal cross-sections of the block, (b) vertical cross-section xOz , and (c) projection of the block contour on the longitudinal yOz plane.

tunnel. When calculating the supporting pressure, the boundary condition on the collapsing (or falling) block surface will be defined as uniform vertical velocity, and zero velocity elsewhere on the surface of the tunnel. The kinematic approach of limit analysis will be used, which does not require calculation of the true stress field, but it needs the construction of a collapse mechanism that will assure the best bound to the calculated safety measure. Collapse mechanisms considered are shown schematically in Fig. 2. The first of the two examples illustrates a block in the shape of a right elliptical cone with a piece-wise linear generatrix. During incipient failure, the block moves downward with uniform vertical velocity. The block in the second example includes a prismatic segment of length l inserted between two halves of the block in Fig. 2(a). Length l defines the maximum length of the collapse mechanism determined by the spacing of the ribs in the tunnel.

3.3. Kinematic approach of limit analysis

A fundamental premise of Limit Analysis is plastic (ductile) behavior of the material. Therefore, application of Limit Analysis to rocks requires a comment, as rocks at low confining stresses exhibit brittle behavior. Chen²¹ argued that the assumption of rock ductility may be questionable, but if the strain of geomaterial is small, and does not reach a brittle drop in stress on the stress-strain deformation curve, then the deformability “may be sufficient to permit the consideration of limit theorems ...” The support for this argument comes from classical experiments indicating some ductility in irreversible behavior prior to collapse of rock specimens.²² Therefore, applications of limit analysis to rocks and concrete can be found in the earlier subject literature.^{23–25}

Application of Limit Analysis theorems requires plastic deformation to be governed by a convex failure criterion and the normality plastic flow rule. The kinematic theorem states that the rate of work dissipation in any kinematically admissible collapse mechanism is not less than the work rate of the true external forces

$$\int_V \sigma_{ij} \dot{\epsilon}_{ij}^{pl} dV + \int_L \sigma_{ij} n_i [v]_j dL \geq \int_S T_i v_i dS + \int_V X_i v_i dV \quad (11)$$

V , S and L are the volume of the mechanism, its boundary surface and the area of the kinematic discontinuities (rupture surfaces), respectively. T_i is the boundary traction vector, σ_{ij} is the stress tensor associated with admissible kinematics, and n_i is the unit vector perpendicular to discontinuity surface L . Vector v_i and $\dot{\epsilon}_{ij}^{pl}$ are the velocity vector in the mechanism and the associated tensor of plastic strain rate, respectively, and $[v]_j$ denotes the velocity discontinuity vector. X_i is the vector of distributed forces, e.g., weight. The theorem in Eq. (11) allows one to calculate an upper bound to a load causing failure of a structure, or a bound to some other measure of stability.

4. Analysis of 3D tunnel roof collapse

4.1. Mechanism with piece-wise linear right elliptical cone block

The first mechanism suggested is the one schematically illustrated in Fig. 2(a). The rock block in this mechanism is generated by a series of n right elliptical cones, each with a different inclination of the generatrix, and with the height defined by co-ordinate h_j , as shown in Fig. 3 ($j = 1, 2 \dots n$). The failure surface separating this block from the stationary rock mass above is then determined by a series of n frustums of right elliptical cones. Consequently, the block has the shape of a right elliptical cone with a piece-wise linear generatrix. In general, an elliptical cone is described by the following equation (origin of the coordinate system in the center of the cone base)

$$\frac{x^2}{a^2} + \frac{y^2}{b^2} = \frac{(z-h)^2}{h^2} \quad (12)$$

where a and b are the half-axes of the base in the x and y directions,

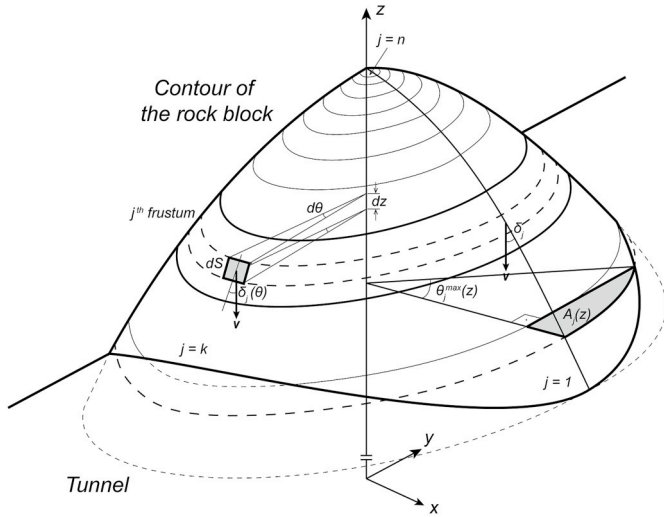


Fig. 4. Right elliptic cone rupture surface and illustration of rupture angle δ_j , infinitesimal surface element dS , maximum integration angle θ_j^{\max} (Eq. (22)), and area A_j (Eq. (24)).

respectively, and h is the cone height. For convenience, Eq. (12) can be transformed for the j th cone into a function of inclination angle α_j of the generatrix defined as $\tan^{-1}(h/a)$

$$x^2 + \frac{y^2}{\lambda^2} = \frac{(z - h_j)^2}{\tan^2 \alpha_j} \quad (13)$$

where λ is ratio b/a , equal for all cones generating the rock block, Fig. 3. It can assume values either smaller or larger than one. When $\lambda = 1$, Eq. (13) defines the right circular cone. Coordinate h_j (Fig. 3(b)) describing the locus of the j th cone apex is

$$h_j = x_j \tan \alpha_j + z_j \quad (14)$$

with z_j being the coordinate of the base of the j th frustum. Ratio λ is not predetermined in the mechanism; rather, it will be found in an optimization effort to find the best bound to the stability measure sought.

Associativity of the plastic flow rule used in limit analysis requires the vertical velocity of the block to be inclined at rupture angle δ (see Fig. 1(b)) to the rupture surface. For a right circular cone surface, this angle is equal to half of the cone apex angle and it is independent of the position on the cone (or frustum). For a right elliptic cone, however, this angle depends on the location on the cone described by angular coordinate θ (Figs. 3(a) and 4). Because the failure surface in the mechanism consists of a series of frustums derived from a series of elliptic cones, each with different generatrix, the rupture angle on the failure surface is a function of angular coordinate θ , and it also will vary from frustum to frustum. Distribution of angle δ on the rupture surface needs to be known in order to calculate the rate of work dissipation during incipient failure. Angle δ at any point M on an elliptical cone failure surface can be calculated as a complementary angle to the angle between the vertical velocity vector and an inward vector perpendicular to the cone surface at point M . Making use of Eq. (A15) in the Appendix and Eq. (13), the rupture angle on frustum j of the mechanism can be written as a function of the locus defined by angular coordinate θ .

$$\delta_j(\theta) = \frac{\pi}{2} - \cos^{-1} \frac{1}{\sqrt{\left(\frac{\cos \theta}{\cot \alpha_j}\right)^2 + \left(\frac{\sin \theta}{\lambda \cot \alpha_j}\right)^2 + 1}} \quad (15)$$

For a right circular cone ($\lambda = 1$), this equation reduces to

$$\delta_j = \frac{\pi}{2} - \alpha_j \quad (16)$$

In order to integrate the rate of work dissipation and the rate of external work, the contour of the cross-section of the circular tunnel and the right elliptic cone block needs to be determined. The circular tunnel cross-section is defined by

$$x^2 + z^2 = R^2 \quad (17)$$

where R is the tunnel radius. The shape of the cross-section of the two surfaces follows directly from Eqs. (13) and (17)

$$\begin{aligned} x(z) &= \sqrt{R^2 - z^2} \\ y(z) &= \lambda \sqrt{\cot^2 \alpha_j (z - h_j)^2 - R^2 + z^2} \end{aligned} \quad (18)$$

This contour forms a 3D curve, which complicates integration of both the rate of work dissipation and the rate of work of the rock weight. The rock block consists of n frustums, fully defined by n angles η_j and n angles α_j (Fig. 3(b)). While the number of frustums n forming the block will be predetermined, specific angles η_j and α_j will be independent variables in the optimization procedure to determine the best bound to the problem solution. The complex shape of the block requires a different integration procedure of work rates for frustums with vertical coordinate $z < R$, a transition frustum, which includes point C (Figs. 3 and 4), and frustums where $z \geq R$. The transition frustum is denoted with index $j = k$, and integration procedures are different for $1 \leq j < k$, $j = k$, and $k < j \leq n$.

Because the blocks shown in Fig. 2 move downward as rigid bodies, the entire effort of the rock is dissipated within a narrow material band separating the blocks from the stationary rock. In calculations, this band will be idealized as a surface, and will be referred to as a failure or rupture surface (or kinematic discontinuity), with the work dissipation rate described in the second term in Eq. (11). The rate of work dissipation per unit area of the rupture surface can be written more specifically as

$$d = v(\tau \cos \delta - \sigma_n \sin \delta) \quad (19)$$

where σ_n and τ are determined in Eqs. (7) and (8), and δ is given in Eq. (15).

Utilizing Eqs. (A3) through (A6) in the Appendix, infinitesimal area element dS of the rupture surface in Fig. 4 can be written as

$$dS = \sqrt{E_j H_j - G_j^2} d\theta dz \quad (20)$$

where E_j , G_j , H_j are defined in the Appendix, Eqs. (A7)–(A9) and angular coordinate θ is shown in Fig. 4. Integrating Eq. (19) over surface S , and utilizing Eq. (15), the following expression was obtained for the total rate of dissipated work

$$\begin{aligned} D = 4v \left\{ \sum_{j=1}^{k-1} \int_{z_j}^{z_{j+1}} \int_0^{\theta_j^{\max}(z)} f_j(z, \theta) d\theta dz + \int_{z_k}^R \int_0^{\theta_k^{\max}(z)} f_k(z, \theta) d\theta dz + \right. \\ \left. \int_R^{z_{k+1}} \int_0^{\pi/2} f_k(z, \theta) d\theta dz + \sum_{j=k+1}^n \int_{z_j}^{z_{j+1}} \int_0^{\pi/2} f_j(z, \theta) d\theta dz \right\} \end{aligned} \quad (21)$$

where

$$\begin{aligned} \theta_j^{\max}(z) &= \tan^{-1} \left(\frac{y(z)}{x(z)} \right) \\ &= \tan^{-1} \left(\lambda \sqrt{\frac{\cot^2 \alpha_j (h_j - z)^2}{R^2 - z^2} - 1} \right), \quad 1 \leq j \leq k \end{aligned} \quad (22)$$

and

$$f_j(z, \theta) = [\tau_j(\theta) \cos \delta_j(\theta) - \sigma_{nj}(\theta) \sin \delta_j(\theta)] \sqrt{E_j H_j - G_j^2} \quad (23)$$

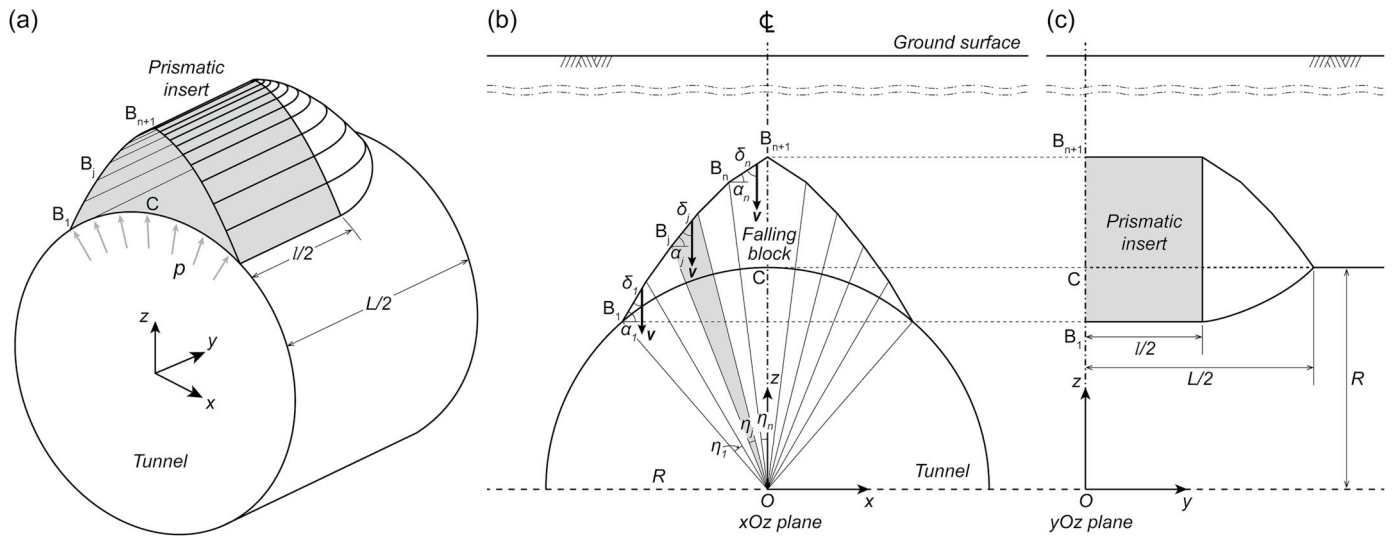


Fig. 6. Right elliptic cone failure block with a prismatic insert: (a) view of a symmetric half of the combined block, (b) cross-section through the insert, and (c) projection of the block contour on vertical plane yOz .

4.2. Mechanism with right elliptical cone and prismatic insert

The mechanism with a block consisting of a series of the right-elliptic frustums can be improved by inserting a prismatic portion between two halves of the potentially unstable block, Fig. 2(b). 2D stability analysis based on a prismatic mechanism was carried out earlier by Park and Michalowski^{2,3} for rocks with strength governed by the Mohr-Coulomb failure criterion with tension cut-off and for the Hoek-Brown criterion. The same procedure is followed in this paper; therefore, the mathematical details of the analysis are not repeated here, but some general comments are offered below.

Shown in Fig. 6 are the view of a symmetrical half of the combined block, the cross-section of its central portion, and the projection of the block on a vertical yOz plane. When combining the prismatic section with the elliptical cone sections, point B_1 and all angles α_j and η_j (and, consequently, all points B_j) need to match those on the central cross-section in the elliptical cone block in Fig. 3. The two halves of the elliptical cone block now form the “caps” of the prismatic portion. In calculating the three measures of stability, the work rate terms for the internal (dissipated) work, work of the rock weight and the work of the resisting pressure from the tunnel lining were included in Eq. (27), in addition to the respective terms for the elliptical cone with the piecewise linear generatrix.

5. Results and discussion

5.1. Optimization

The analysis approach taken yields an upper bound to factor of safety F , and lower bounds to stability number N and required support pressure $p/\gamma R$. The specific geometry of the falling block is not pre-determined in calculations. An optimization process is used to arrive at the geometry that yields the best bound to the required stability measure. The independent variables in the optimization of the piece-wise linear right elliptical block mechanism are: n angles α_j and n angles η_j , where n is the number of frustums in the block (the number of linear sections in the block generatrix, Fig. 3). In addition, ratio λ of the half-axes in the elliptical base of the conical surfaces is a variable ($\lambda = 1$ for a circular base conical block). Calculations were performed in the Matlab environment. In the process of optimization, all angles were varied with minimum increments of 0.01° (starting at 1°), and ratio λ was varied with a minimum step of 0.001. The process is subject to a constraint on the total length of the mechanism, given by ratio L/R (mechanism

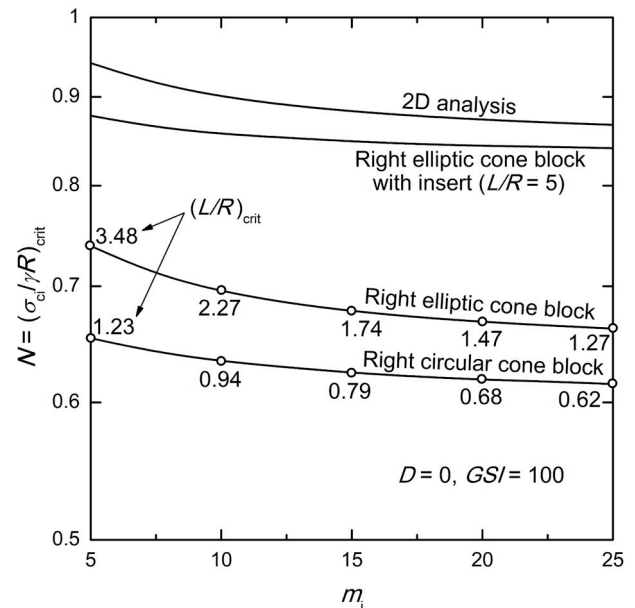


Fig. 7. Stability number $N = (\sigma_{ci}/\gamma R)_{crit}$ as a function of m_i for roof failures in circular tunnels from four analyses with different collapse blocks ($D = 0$, $GSI = 100$).

length/tunnel radius). The length limitation is governed by the spacing of the ribs in the tunnel. The process of optimization was carried out until the difference in the calculated measure of stability in the two consecutive loops was less than 10^{-6} . The number of frustums in the block shape description was 15 (an improvement in the results due to an increase in the number of frustums beyond 15 was less than 0.1%). The length of the prismatic insert (if used) was not an independent variable. The length of the critical mechanism with a prismatic insert always reached the length constraint ratio L/R ; the length of the insert was then calculated as a complementary length to the length of the elliptical cone portion of the mechanism.

5.2. Results of calculations

Stability numbers from analyses with four different mechanisms

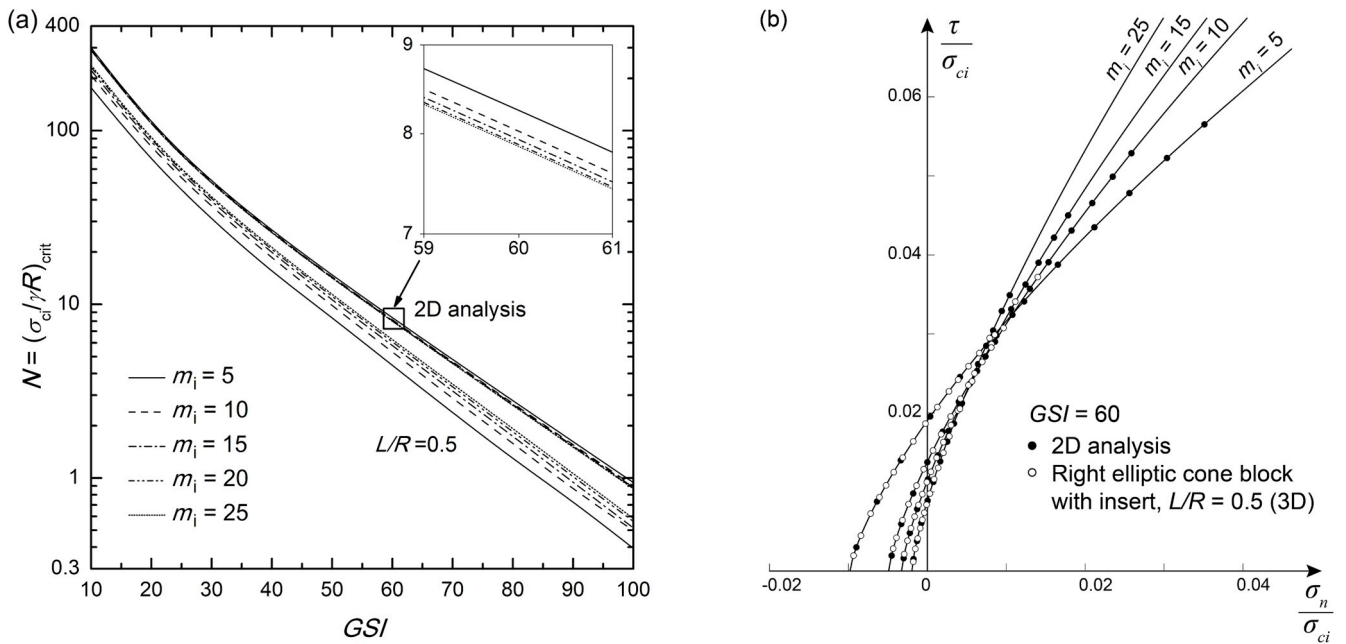


Fig. 8. (a) Stability number as function of GSI ($D = 0$) from 2D analysis and the right elliptic cone block with prismatic insert and constraint $L/R = 0.5$, and (b) back-calculated stress range on the rupture surface from 2D and 3D analyses.

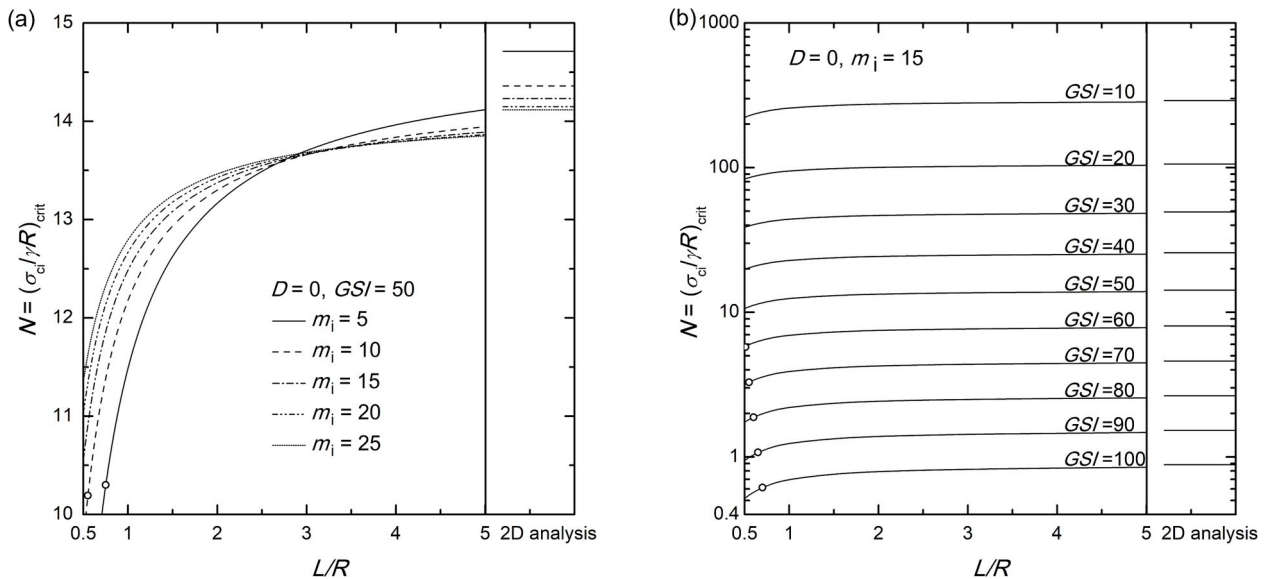


Fig. 9. Stability number for circular tunnel roofs as a function of collapse block length ratio L/R : (a) the influence of coefficient m_i , and (b) the influence of GSI .

(block shapes) are shown in Fig. 7 as functions of rock type coefficient m_i , for $GSI = 100$ and a disturbance factor of 1. The constraint for the length of the mechanism is $L/R = 5$ (except in the 2D analysis). The higher the stability number, the more conservative the assessment of safety. Not surprisingly, the most conservative is the 2D analysis, followed by the mechanism with the elliptic base block with a prismatic insert. The latter mechanism reaches a length constraint of $L/R = 5$ for every coefficient m_i . The optimized mechanisms with either the right circular or the right elliptic block mechanism did not reach the length constraint, and length $(L/R)_{crit}$ for which the stability number was attained was part of the solution, marked as circular bullets on the chart. The elliptic cone block with the plane insert will be used to produce the computational data for the remaining charts and tables. A block without a plane insert is a special case of this mechanism, and only in rare cases, for very small constraint L/R , the critical mechanism included no insert.

The impact of the 3D analysis on the stability number is illustrated in Fig. 8 for a length constraint of $L/R = 0.5$. Even with this very stringent length constraint, the critical mechanisms contained a plane insert for most of the parametric range used. The plane strain analysis shows the results very much dependent on GSI but almost independent of coefficient m_i describing the type of rock. The 3D analysis shows a more distinct dependence on the type of rock, but this dependence is counterintuitive; the roof in the rock with lower m_i appears to be more stable (lower N) than roofs in the rocks with higher m_i . This trend changes, however, with an increase in the mechanism length constraint. With an increase in L/R , the curves for all coefficients m_i come closer together, and the trend becomes opposite for 2D analysis (see insert in Fig. 8(a)). The plausible reason for this change in the trend can be deduced from Fig. 8(b), where the Hoek-Brown strength envelope is plotted for different coefficients m_i . The rocks with low coefficient m_i have generally

Table 1
Stability numbers for roofs in circular tunnels from 3D analysis ($D = 0$).

L/R	m_i	Geological Strength Index GSI				
		20	40	60	80	100
0.5	5	66.95	15.33	4.44	1.28	0.39
	15	83.37	19.79	5.77	1.73	0.51
	25	88.15	21.09	6.26	1.92	0.58
0.6	5	74.26	17.49	4.87	1.47	0.46
	15	87.26	20.86	6.18	1.89	0.57
	25	91.22	21.88	6.56	2.04	0.63
0.8	5	83.46	19.85	5.81	1.75	0.54
	15	92.23	22.15	6.67	2.09	0.65
	25	94.93	22.85	6.93	2.19	0.69
1	5	88.65	21.26	6.36	1.97	0.61
	15	95.11	22.90	6.96	2.20	0.70
	25	97.09	23.42	7.14	2.28	0.73
1.5	5	95.66	23.07	7.05	2.25	0.72
	15	98.84	23.90	7.33	2.36	0.76
	25	99.90	24.17	7.43	2.39	0.77
2	5	99.04	23.97	7.39	2.39	0.78
	15	100.62	24.38	7.51	2.43	0.79
	25	101.28	24.54	7.56	2.45	0.80
3	5	102.33	24.84	7.71	2.52	0.83
	15	102.38	24.85	7.69	2.50	0.82
	25	102.63	24.90	7.70	2.50	0.82
5	5	104.78	25.53	7.97	2.63	0.87
	15	103.80	25.23	7.82	2.56	0.84
	25	103.67	25.18	7.81	2.54	0.84
2D analysis	5	108.58	26.55	8.36	2.78	0.94
	15	105.94	25.79	8.04	2.64	0.88
	25	105.33	25.62	7.97	2.61	0.86

lower shear strength in the compressive regime, but they have higher tensile strength and higher shear strength at low normal stresses than rocks with larger m_i . The limit stress back-calculated from the analyses is indicated as filled bullets for the 2D analysis and open bullets for the 3D analysis. It appears that the stress in the 3D analysis spans the range where rocks with lower coefficient m_i have higher shear strength than rocks with larger m_i , causing the unexpected effect. The trend is reversed in the 2D analysis. Limit analysis is an approximate method, thus stresses back-calculated from the critical mechanism are not the true stresses, but they can be used to explain the trends in limit analysis

solutions.

The influence of the length constraint on the stability number is illustrated in Fig. 9(a). The stability number increases (the tunnel roof becomes less stable) with an increase in the mechanism length; this is consistent with expectations (the smaller the spacing of ribs in the tunnel, the more stable the roof). For rocks with $GSI = 50$ and $D = 0$, and mechanism length constraint $L/R < 3$, the increase in coefficient m_i has a destabilizing effect, but for larger lengths, this trend is reversed. The dependence of the stability number on GSI is illustrated in Fig. 9(b) in the semi-log scale. Both Fig. 9(a) and (b) clearly indicate that constraining the length of the failure mechanism has an effect of increased safety (stabilizing effect). It was interesting to notice that critical mechanisms for most of the combination of the rock parameters and mechanism length constraint contained the plane insert. The open bullets on the curves in the charts indicate points where for smaller constraint L/R , the optimized mechanism did not have a plane insert. For comparative purposes, selected numerical results are presented in Table 1.

Calculated factors of safety are illustrated in Fig. 10 in semi-log scale, as functions of the characteristic strength number $\sigma_{ci}/\gamma R$. The graph includes F -functions for various GSI and mechanism length constraint L/R

Table 2
Factors of safety for roofs in circular tunnel from 3D analysis ($D = 0$).

$\sigma_{ci}/\gamma R$	GSI	m_i	L/R						
			0.5	0.6	0.8	1	2	2D analysis	
100	20	5	1.35	1.32	1.20	1.10	1.10	0.95	
		15	1.11	1.08	1.04	1.02	0.99	0.97	
		25	1.09	1.08	1.06	1.05	1.02	0.97	
	40	5	5.97	4.56	3.32	2.99	2.69	2.16	
		15	2.90	2.73	2.51	2.38	2.19	2.05	
		25	2.74	2.61	2.44	2.36	2.21	2.03	
	10	60	5	1.95	1.66	1.50	1.46	1.23	1.11
			15	1.40	1.34	1.27	1.23	1.16	1.12
			25	1.39	1.31	1.26	1.24	1.20	1.12
80		5	5.48	4.76	4.14	3.66	2.98	2.26	
		15	3.63	3.26	2.88	2.67	2.32	2.10	
		25	3.06	2.93	2.70	2.54	2.31	2.06	
1	100	5	1.99	1.81	1.58	1.45	1.24	1.04	
		15	1.49	1.41	1.31	1.24	1.14	1.07	
		25	1.43	1.40	1.28	1.25	1.18	1.08	

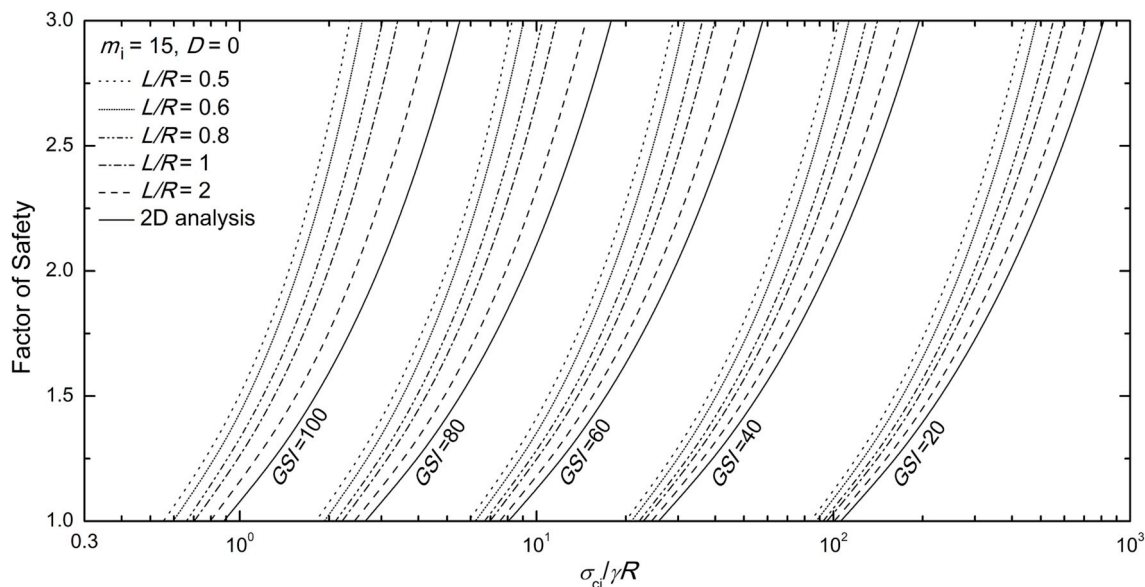


Fig. 10. The factor of safety as a function of characteristic strength number $\sigma_{ci}/\gamma R$ and collapse block length ratio L/R .

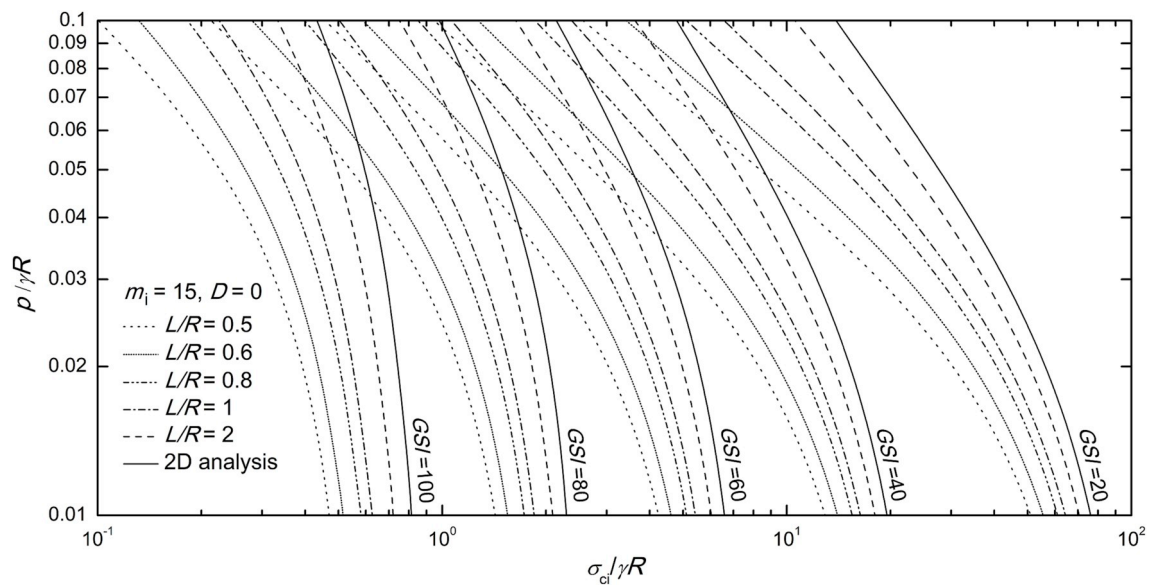


Fig. 11. Required supporting pressure (dimensionless) for tunnel with different length-to-radius ratios L/R as function of the characteristic strength number.

Table 3
Required roof supporting pressure ($p/\gamma R \times 10^3$) for circular tunnels from 3D analysis ($D = 0$).

$\sigma_{ci}/\gamma R$	GSI	m_i	L/R					2D analysis
			0.5	0.6	0.8	1	2	
10	20	5	90.35	107.54	143.47	174.87	269.95	485.32
		15	45.36	52.92	66.00	76.66	104.85	138.35
		25	32.42	37.18	44.87	50.55	64.04	78.62
	40	5	27.27	34.60	47.90	58.39	84.77	141.17
		15	15.94	18.74	23.10	26.12	33.18	40.98
		25	11.61	13.20	15.49	17.02	20.32	23.73
1	60	5	109.67	128.71	188.62	233.17	445.18	904.84
		15	57.56	66.34	89.15	103.65	164.41	253.37
		25	42.26	49.32	61.88	72.31	101.52	140.33
	80	5	39.23	51.11	77.38	100.15	177.87	358.51
		15	24.77	30.26	40.21	48.16	70.28	98.34
		25	18.63	22.23	28.11	32.49	43.11	55.27
0.1	100	5	198.09	252.67	351.89	460.32	926.52	2393
		15	100.42	123.87	162.44	200.85	370.38	704.11
		25	75.41	90.59	116.43	139.97	153.87	389.27

R ($m_i = 15, D = 0$). If the characteristic strength number for a given tunnel is equal to the stability number, the factor of safety becomes equal to one. The balance of work rate in Eq. (27) leads to an implicit equation with respect to F , and an iterative process was used to arrive at the solution (Matlab built-in procedure was used for this purpose). As expected, the factor of safety increases with an increase of the rock characteristic strength number and with a decreasing length constraint L/R . Selected results are presented in Table 2.

The outcome of calculations of the roof supporting pressure required to maintain equilibrium (prevent collapse) is shown in Fig. 11 in log-log scale, as a function of the characteristic strength number $\sigma_{ci}/\gamma R$. Supporting pressure is needed always when the characteristic strength number is lower than the stability number. The lower the characteristic strength number, the larger the support pressure needed. For a given rock, the required support pressure increases with an increase of the mechanism length described by the length constraint L/R . As expected, the larger the GSI the lower the support pressure needed. The charts are given for $m_i = 15$, but the same trend is found for other types of rock. For comparative purposes, selected numerical results are presented in Table 3.

To the best of the author’s knowledge, the results presented are the

first of its kind for three-dimensional roof collapse mechanisms in tunnels with a circular cross-section. For that reason, the authors were unable to compare the outcome to other results.

6. Conclusions

Roof collapse is a common failure mode in tunnels. The kinematic approach of limit analysis was used in order to calculate three measures of safety: the stability number, the factor of safety, and the support pressure required to maintain stability. The rock strength is described by the Hoek-Brown failure criterion, and the rock block considered in the failure mechanism consists of a right elliptical cone with a piece-wise linear generatrix, and a prismatic section inserted between the two halves of the cone. Deep tunnels were considered, with the failure mechanism not propagating to the ground surface. An intersection of this rock block with the circular cross-section tunnels makes a complex shape and leads to an intricate integration of the rates of work dissipation and the work of external forces in the mechanism during incipient collapse.

Because the original form of the Hoek-Brown criterion is a function of principal stresses, an alternative form of the criterion is often used in

geomechanics analyses that call for an explicit dependence of the shear strength on the normal stress. This issue was circumvented in this paper by using a parametric form of the original Hoek-Brown function.

Not surprisingly, the outcome of the analysis is strongly dependent on the quality of the rock, described by the Geologic Strength Index in the Hoek-Brown failure criterion. Dependence on the rock type represented by coefficient m_i is less distinct, with a trend that is not necessarily unique. A restriction on the length of the collapse mechanism (falling block) was introduced in the analysis to account for the presence of the strong ribs supporting the tunnel; the mechanism was restrained to the length between the neighboring ribs. All measures of safety strongly depend on the rib spacing; the safety of the tunnel against roof collapse increases with a decrease in the spacing between the ribs.

Appendix

A.1. Right elliptic cone

The right elliptic cone is described in Eq. (12). The volume of the elliptic cone is determined by

$$V = \frac{\pi}{3}abh \quad (\text{A1})$$

The lateral surface area of the right elliptic cone is calculated by introducing the form²⁶

$$x = a \frac{h-u}{h} \cos v, \quad y = b \frac{h-u}{h} \sin v, \quad z = u \quad (\text{A2})$$

where $0 \leq u \leq h$ and $0 \leq v < 2\pi$. The lateral surface area of the right elliptic cone is obtained as

$$S = \int_0^{2\pi} \int_0^h \sqrt{EH - G^2} du dv \quad (\text{A3})$$

where E , G , and H are defined as

$$E = \frac{h^2 + a^2 \cos^2 v + b^2 \sin^2 v}{h^2} \quad (\text{A4})$$

$$G = \frac{(a^2 - b^2)(h-u) \cos v \sin v}{h^2} \quad (\text{A5})$$

$$H = \frac{(h-u)^2 (a^2 \sin^2 v + b^2 \cos^2 v)}{h^2} \quad (\text{A6})$$

Above coefficients now can be specified for the j th frustum of the mechanism as

$$E_j(\theta) = 1 + \cot^2 \alpha_j (\cos^2 \theta + \lambda^2 \sin^2 \theta) \quad (\text{A7})$$

$$G_j(z, \theta) = (h_j - z) \cot^2 \alpha_j (1 - \lambda^2) \cos \theta \sin \theta \quad (\text{A8})$$

$$H_j(z, \theta) = (h_j - z)^2 \cot^2 \alpha_j (\sin^2 \theta + \lambda^2 \cos^2 \theta) \quad (\text{A9})$$

Sector area A of an ellipse, Fig. A1, between two angles θ_1 and θ_2 , is defined as

$$A = F(\theta_2) - F(\theta_1) \quad (\text{A10})$$

where

$$F(\theta) = \frac{ab}{2} \left[\theta - \tan^{-1} \left(\frac{(b-a) \sin 2\theta}{(b+a) + (b-a) \cos 2\theta} \right) \right] \quad (\text{A11})$$

A.2. Angle between a vertical and a plane tangent to an elliptic cone

The direction of block velocity is given by the unit vector

$$\vec{m} = (0, 0, -1) \quad (\text{A12})$$

A tangent plane to a right elliptic cone along a generatrix containing point $M(x_M, y_M, z_M)$ is (Fig. A1)

$$\frac{2x_M}{a^2}(x-x_M) + \frac{2y_M}{b^2}(y-y_M) - \frac{2(h-z_M)}{h^2}(z-z_M) = 0 \tag{A13}$$

and a vector normal to that plane at point M is determined as

$$\vec{n} = \left(\frac{2x_M}{a^2}, \frac{2y_M}{b^2}, -\frac{2(h-z_M)}{h^2} \right)$$

or

$$\vec{n} = \left(x_M, \frac{y_M}{\lambda^2}, -\frac{h-z_M}{\tan^2 \alpha} \right) \tag{A14}$$

Angle χ between vectors \vec{n} and \vec{m} , Fig. A1, is thus given by the following expression

$$\cos \chi = \frac{|\vec{n} \times \vec{m}|}{\|\vec{n}\| \|\vec{m}\|} = \frac{\frac{h-z_M}{\tan \alpha^2}}{\sqrt{x_M^2 + \left(\frac{y_M}{\lambda^2}\right)^2 + \left(-\frac{h-z_M}{\tan^2 \alpha}\right)^2}}$$

$$= \frac{1}{\sqrt{\left(\frac{\cos \theta}{\cot \alpha}\right)^2 + \left(\frac{\sin \theta}{\lambda \cot \alpha}\right)^2 + 1}} \tag{A15}$$

Consistent with the normality flow rule, rupture angle δ is the angle between the velocity of the block and the elliptic cone failure surface, and is the complementary angle to angle χ ($\delta = \pi/2 - \chi$).

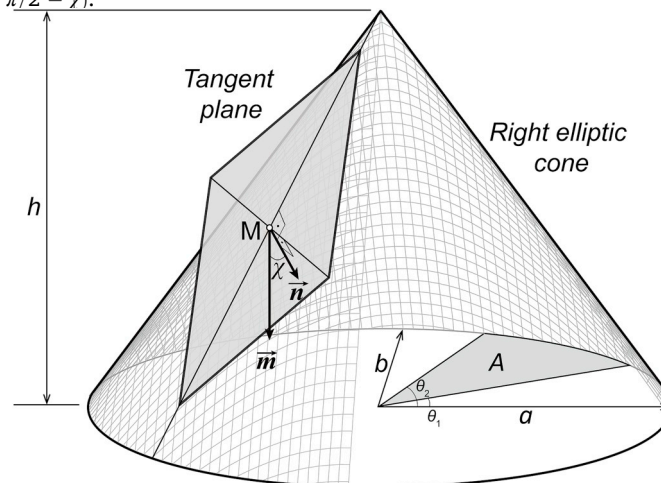


Fig. A1. Angle χ between velocity direction \vec{m} and normal to the rupture surface \vec{n} at point $M(x_M, y_M, z_M)$.

References

- 1 Fraldi M, Guarracino F. Limit analysis of collapse mechanisms in cavities and tunnels according to the Hoek–Brown failure criterion. *Int J Rock Mech Min Sci.* 2009;46(4): 665–673.
- 2 Park D, Michalowski RL. Tunnel roof stability in soft rock with tension cutoff. In: *GeoShanghai International Conference, Shanghai.* 27–30 May 2018:361–368.
- 3 Park D, Michalowski RL. Roof stability in deep rock tunnels. *Int J Rock Mech Min Sci.* 2019;124:1–12, 104139.
- 4 Lippmann H. Plasticity in rock mechanics. *Int J Mech Sci.* 1971;13(4):291–297.
- 5 Sloan S, Assadi A. *Stability of Shallow Tunnels in Soft Ground.* Predict Soil Mech London: Thomas Telford; 1993:644–663.
- 6 Abbo AJ, Wilson DW, Sloan SW, Lyamin AV. Undrained stability of wide rectangular tunnels. *Comput Geotech.* 2013;53:46–59.
- 7 Fraldi M, Guarracino F. Analytical solutions for collapse mechanisms in tunnels with arbitrary cross sections. *Int J Solid Struct.* 2010;47(2):216–223.
- 8 Fraldi M, Cavuoto R, Cutolo A, Guarracino F. Stability of tunnels according to depth and variability of rock mass parameters. *Int J Rock Mech Min Sci.* 2019;119:222–229.
- 9 Yang X, Huang F. Three-dimensional failure mechanism of a rectangular cavity in a Hoek–Brown rock medium. *Int J Rock Mech Min Sci.* 2013;61:189–195.
- 10 Huang F, Yang X, Ling T. Prediction of collapsing region above deep spherical cavity roof under axis-symmetrical conditions. *Rock Mech Rock Eng.* 2014;47(4): 1511–1516.
- 11 Hoek E, Carranza-Torres C, Corkum B. Hoek–Brown failure criterion-2002 edition. *Proc NARMS Tac.* 2002;1:267–273.
- 12 Paul B. A modification of the Coulomb–Mohr theory of fracture. *J Appl Mech.* 1961;28 (2):259–268.
- 13 Bieniawski ZT. Estimating the strength of rock materials. *J S Afr Inst Min Metall.* 1974;74(8):312–320.
- 14 Barton N. The shear strength of rock and rock joints. *Int J Rock Mech Min Sci.* 1976;13 (9):255–279.
- 15 Hoek E, Brown ET. Empirical strength criterion for rock masses. *J Geotech Eng Div.* 1980;106(9):1013–1035.
- 16 Hoek E, Marinos P. A brief history of the development of the Hoek–Brown failure criterion. *Soils Rocks.* 2007;2(November):1–13.
- 17 Marinos P, Hoek EGSL. A geological friendly tool for rock mass strength estimation. In: *International Conference on Geotechnical and Geological Engineering.* Melbourne: GeoEng; 2000:1422–1446.
- 18 Michalowski RL, Park D. Stability assessment of slopes in intact rock governed by the Hoek–Brown strength criterion. *Int J Rock Mech Min Sci.* 2020;127:1–12, 104217.
- 19 Balmer G. A general analysis solution for Mohr’s envelope. *Proc ASTM.* 1952;52: 1260–1271.
- 20 Kumar P. Shear failure envelope of Hoek–Brown criterion for rockmass. *Tunn Undergr Space Technol.* 1998;13(4):453–458.
- 21 Chen W-F. *Limit Analysis and Soil Plasticity.* New York: Elsevier; 1975.
- 22 Swanson SR, Brown WS. The influence of state of stress on the stress-strain behavior of rocks. *J Basic Eng.* 1972;94(1):238–242.
- 23 Chen WF, Drucker DC. Bearing capacity of concrete blocks or rock. *J Eng Mech Div.* 1969;95(4):955–978.
- 24 Michalowski R. Limit analysis of quasi-static pyramidal indentation of rock. *Int J Rock Mech Min Sci.* 1985;22(1):31–38.
- 25 Nielsen MP. *Limit Analysis and Concrete Plasticity.* 2 ed. New York: CRC Press; 1998.
- 26 Weinsstein E. *Elliptic Cone*, 2019. <http://mathworld.wolfram.com/EllipticCone.html>.